

$0f_{7/2}$ proton transfer on ^{55}Mn R. T. Newman,¹ R. W. Fearick,² S. M. Perez,² D. G. Aschman,² K. Bharuth-Ram,³ W. A. Richter,⁴ F. D. Smit,¹
V. M. Tshivhase,² and T. S. Volkwyn²¹National Accelerator Centre, Faure, 7131, South Africa²Department of Physics, University of Cape Town, Rondebosch, 7700, South Africa³Department of Physics, University of Durban-Westville, Durban, 4000, South Africa⁴Department of Physics, University of Stellenbosch, Stellenbosch, 7600, South Africa

(Received 10 April 1996)

Proton pickup data have been obtained through the $^{55}\text{Mn}(d,^3\text{He})^{54}\text{Cr}$ ($E_d = 46$ MeV) reaction in the 6° – 30° angular range using a magnetic spectrometer with a resolution of ~ 40 keV full width at half maximum. Spectroscopic factors associated with transitions to 24 ^{54}Cr final states ($E^* \leq 6.104$ MeV) were determined from local, zero-range distorted-wave Born approximation analyses of the measured angular distributions allowing for $\ell = 0, 1, 2,$ and 3 transfer. A spin-dependent sum-rule analysis of the $0f_{7/2}$ proton transfer data has been performed using complementary stripping data from a study of the $^{55}\text{Mn}(\alpha,t)^{56}\text{Fe}$ reaction. The $0f_{7/2}$ proton transfer data have also been compared to results from a $0f_{1p}$ shell-model calculation based on a new effective interaction for $A = 41$ – 66 nuclei. [S0556-2813(96)05109-6]

PACS number(s): 25.45.Hi, 21.10.Jx, 21.60.Cs, 24.10.Eq

I. INTRODUCTION

The analysis of spin distributions of spectroscopic strength associated with one-nucleon pickup and stripping on odd-even fp shell nuclei by means of nonenergy weighted sum rules (NEWSR) continues to be of interest. A recent innovation has been the introduction of a normalization procedure based on the symmetric form of the NEWSR [1]. This has been successfully applied to a study of $0f_{7/2}$ single-proton transfer data on ^{51}V and ^{59}Co , and has pointed out the possibility that the spin distribution of high-lying spectroscopic strength is proportional to $(2J' + 1)$, where J' is the final state spin [1].

NEWSR analyses have mostly been performed on $0f_{7/2}$ transfer data acquired in the lower part of the fp shell [2]. This is because the large energy gap between the $0f_{7/2}$ and $0f_{5/2}$ orbitals allows a confident assignment of $0f_{7/2}$ to any $\ell = 3$ transition to a low excitation energy final state in this mass region. The chosen target should have as high a ground-state spin J_t as possible, since for an angular momentum transfer j , the number of linear relations constituting the NEWSR is equal to $\min\{[J_t],[j]\}$ where $[x] = (2x + 1)$ [2]. Thus, the larger J_t , the greater the number of linear relations representing the NEWSR, and the greater the overdeterminacy of any quantity to be determined through the sum rules (e.g., the normalization n in Sec. IV B). A NEWSR analysis requires the spin distributions of transfer strength for one-nucleon stripping and pickup on the same nucleus [2]. Before the present work, ^{47}Ti and ^{55}Mn were the only remaining targets in the lower part of the fp shell with $J_t \geq \frac{5}{2}$ for which NEWSR analyses had not been performed [1,2]. We focus on the second of these targets in this study.

Two earlier studies of proton stripping on ^{55}Mn exist. The first study was performed by Hinrichsen and Rosner who employed the $(^3\text{He},d)$ reaction and studied transitions to only three ^{56}Fe final states [3]. No spectroscopic factors were reported. A more extensive study [4] was undertaken by Ma-

toba who used the (α,t) reaction to study transitions to twelve ^{56}Fe final states. Spectroscopic factors associated with transitions to seven of these states were reported. These data, in conjunction with the adopted ^{56}Fe final state spins [5,6], are tabulated in Table I.

Two previous studies also exist of proton pickup on ^{55}Mn . In the first, Colli *et al.* [7,8] reported transitions to five final states observed via the (n,d) reaction. However, they only derived the spectroscopic factor for the transition to the ^{54}Cr ground state. The second study, by Yntema *et al.* [9], who employed the $(d,^3\text{He})$ reaction, yielded no spectroscopic factors.

A reliable set of spectroscopic factors for $0f_{7/2}$ proton pickup on ^{55}Mn was therefore needed. In the present study these were obtained through distorted-wave Born approximation (DWBA) [10] analyses of the differential cross section for the $^{55}\text{Mn}(d,^3\text{He})^{54}\text{Cr}$ reaction at a beam energy of 46 MeV. This beam energy was chosen so as to exploit available parametrizations of the mass dependence of optical potentials for ^3He at 39 MeV [11] and 41 MeV [12], and thus to determine distorted-wave functions for the exit channel. The form of the optical potential used to generate the distorted waves for the entrance channel was identical to one used to obtain a global parametrization of deuteron optical model parameters [13]. An analysis of the angular distribution for the $^{55}\text{Mn}(d,d)^{55}\text{Mn}(\text{g.s.})$ ($E_d = 46$ MeV) reaction was made in order to obtain optimum parameters for this potential.

Recently, a shell-model calculation has been performed for $A = 41$ – 66 nuclei, using a new two-body effective interaction and a model space which allows for the excitation of a $0f_{7/2}$ particle to the $1p_{3/2}$, $0f_{5/2}$, and $1p_{1/2}$ subshells [14]. Theoretical energy levels and static electromagnetic moments have been shown to be in good agreement with their experimental counterparts [14]. In order to further assess the quality of this calculation the derived wave functions were used to calculate spectroscopic factors to be compared

TABLE I. Spectroscopic information on $\ell = 3$ stripping strength from the $^{55}\text{Mn}(\alpha, t)^{56}\text{Fe}$ reaction as reported by Matoba [4]. The possible ^{56}Fe adopted levels [5,6] which correspond with observed states reached via $\ell = 3$ transfer are shown. J_t and J' denote target ground and final state spin, respectively.

From Refs. [5,6]			From Ref. [4]			
E^*	ΔE^*	$J' \pi$	E^*	ΔE^*	ℓ	$\frac{[J']}{[J_t]} C^2 S$
(MeV)	(keV)		(MeV)	(keV)		
0.0		0^+	0		3	0.01
0.847	< 1	2^+	0.85		3	1.45
2.085	< 1	4^+	2.09		3	0.36
2.658	< 1	2^+	2.66		3	0.14
2.942	< 1	0^+				
2.960	< 1	2^+				
			2.97 ^a	40	3	0.04
3.070	30	(3^-)				
3.120	< 1	(1^+)				
3.123	< 1	4^+				
			3.15 ^a	40	3	0.04
3.370	< 1	2^+				
3.388	< 1	6^+				
			3.40	40	3	0.90
3.748	5	2^+				
3.756	< 1	6^+				
3.760	10	$(2-6)$				
			3.78	40	3	0.25
3.832	< 1	2^+				

^aMember of the state complex observed at (2.97 + 3.15) MeV with a combined $\ell = 3$ strength of 0.08.

with those determined through single-proton transfer on ^{55}Mn .

The experimental methods used to collect the pickup and elastic scattering data are discussed in Sec. II. The extraction of angular distributions from these data and the subsequent calculation of spectroscopic factors via DWBA analyses are described in Sec. III. In Sec. IV we first outline the results of the shell-model calculation after which we describe how the stripping and pickup spin distributions for $0f_{7/2}$ proton transfer strength were established. Nonenergy weighted and dipole sum-rule analyses of these spin distributions are then described. A concluding summary is presented in Sec. V.

II. EXPERIMENTS

The differential cross sections for the $^{55}\text{Mn}(d, ^3\text{He})^{54}\text{Cr}$ and $^{55}\text{Mn}(d, d)^{55}\text{Mn}(\text{g.s.})$ reactions at $E_d = 46$ MeV were measured at the National Accelerator Centre (NAC) [15,16], Faure, South Africa. A recently commissioned $k = 600$ MeV magnetic spectrometer similar in design to the K600 magnetic spectrometer at the Indiana University Cyclotron Facility [17] was used. The reaction products were detected in a focal-plane detector array consisting of a vertical drift chamber (VDC) followed by two plastic scintillation counters.

The VDC negative high voltage planes comprised two 27 μm Al foils separated by 16.0 mm. A wire plane comprising 198 earthed signal wires, each 25 μm thick and 4.0 mm apart, interspersed by 199 guard wires each of thickness 50 μm , was situated midway between these foils. All wires were made from Au-plated tungsten. The VDC was operated

with negative high voltages of 3.50 kV and 550 V applied to the foils and guard wires, respectively, while using a 90% Ar/10% CO_2 gas mixture at atmospheric pressure.

In the following the first scintillator will be called paddle 1 and the next one paddle 2. These were 3.2 mm and 12.7 mm thick, respectively. When acquiring elastic scattering data, i.e., operating the spectrometer in the (d, d) mode, paddle 1 was operated in coincidence with paddle 2 in order to generate an event trigger. For a beam energy of 46 MeV, helions (^3He particles) associated with an excitation energy of up to 6 MeV in ^{54}Cr were stopped inside paddle 1. Paddle 2 was therefore operated in anticoincidence with paddle 1 to reduce the noise background when acquiring pickup data in the $(d, ^3\text{He})$ mode.

Data were collected at spectrometer angles θ varying between 6° and 50° in 2° steps by operating the spectrometer in a normal angle mode ($\theta \geq 18^\circ$) and a small angle mode ($6^\circ \leq \theta \leq 18^\circ$). When operating in the normal angle mode the deuteron beam was stopped in an external Faraday cup, while a 40 mm thick graphite block served as an internal beam stop in the small angle mode. The latter arrangement gave rise to a high background in the 301 mm diameter scattering chamber used, ruling out the use of a monitor detector to check the consistency of the charge collection.

A 20 mm thick brass collimator with a vertical aperture of 14×55 mm defined the acceptance of the spectrometer. The back edge of the collimator was located 735.5 mm from the center of the target. This gave an in-plane (horizontal) angular acceptance of 1.09° and an out-of-plane (vertical) acceptance of 4.28° .

The deuteron beam was produced with the NAC $k = 8$ MeV solid-pole light-ion injector cyclotron, accelerated to 4 MeV, and then injected into the separated-sector cyclotron and further accelerated to a nominal energy of 46 MeV. No pulse selection was used since the associated beam-burst period of 101.2 ns facilitated particle identification (PID) via time of flight as discussed below. Slits were used to keep the energy spread to ~ 10 keV. The beam halo was reduced by tuning the beam in order to minimize the paddle count rate from an empty target frame. In this manner it was possible to reduce the halo rate down to $\leq 4\%$ of the count rate obtained with the target in place. An achromatic beam varying in intensity between 1 and 29 nA was used to collect the pickup and elastic scattering data. The accumulated charge associated with pickup data sets varied between 96 and 506 μC , while that for elastic scattering varied between 0.02 and 48 μC .

The target consisted of a layer of 99.9% pure ⁵⁵Mn evaporated onto a 1.5 μm thick Mylar backing. Layer thicknesses were measured using Rutherford backscattering spectrometry (RBS) performed at the Van de Graaff facility at the NAC. The full width at half maximum (FWHM) of the ⁵⁵Mn peak, in conjunction with stopping powers, was used to determine the thickness of the deposited layer by simulation of the RBS spectrum with the computer program RUMP [18]. Two targets having ⁵⁵Mn layer thicknesses of 159 and 235 $\mu\text{g cm}^{-2}$, respectively, were used in this work. The uncertainty (1σ) associated with these thicknesses was estimated by nonstatistical means [19] to be 5%.

Standard electronics were used to process the paddle and cyclotron radio-frequency (rf) signals in order to, among others, generate an event trigger. VDC wire signals were processed by a LeCroy 4290 drift chamber readout system. The effective dead time was monitored using a clock and two scalars, one of which was inhibited by the busy signal associated with the focal-plane electronics. While acquiring data the dead time was typically 4% but never more than 11%. Digitized paddle pulse heights, time of flight, VDC drift times, and scalar information were interfaced with a VAX-11/750 computer by means of a microprogrammable branch driver. The data acquisition and analysis software package XSYS [20,21] was used to process these data which were also written to tape in an event-by-event format for off-line analysis.

The time of flight (TOF) through the spectrometer of the rigidity selected reaction products facilitated particle identification. The start signal for the TOF measurement was obtained from the paddles operated in mean-timing mode, while the stop signal was generated from the rf signal. A typical TOF spectrum acquired in the ($d, ^3\text{He}$) mode showing the location of the helion peak, among the other particle peaks, can be seen in Fig. 1. The helion TOF peak width, calculated using extreme path lengths through the spectrometer, also shown in Fig. 1, corresponds well with the measured widths. The helion peak was always well separated from the other TOF structure, obviating the need for an additional means of particle identification. A single TOF peak associated with the deuterons of interest was observed when acquiring the elastic scattering data. This is because all particles with the same rigidity as the deuterons of interest were stopped in the materials constituting the focal-plane detector

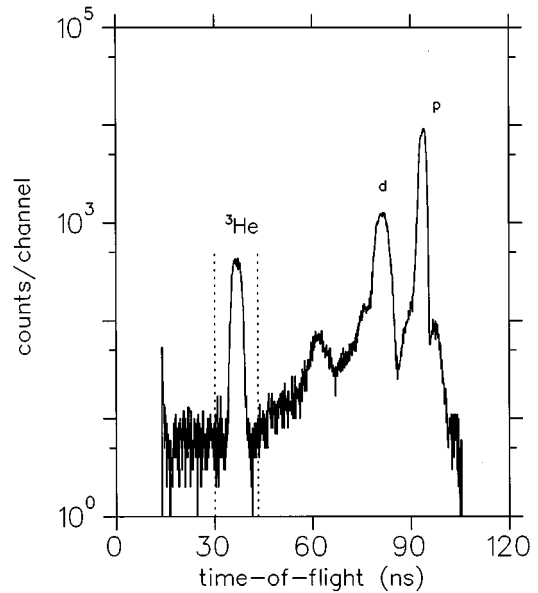


FIG. 1. A typical spectrum of the time of flight through the spectrometer associated with rigidity-selected charged reaction products while acquiring pickup data. The timing start signal was derived from the paddle plastic scintillation detectors while the stop signal was generated from the cyclotron rf signal.

array, resulting in no further PID being required while operating the spectrometer in the (d, d) mode.

III. DATA ANALYSIS

A. Data reduction

Focal-plane position spectra associated with helion and deuteron events of interest were generated via off-line analyses of acquired event-by-event data. These events were selected by first setting a gate on the relevant peak in the TOF spectrum. VDC data (drift times and wire numbers) associated with each event which fell in the selected TOF peak were checked to ascertain whether drift times fell within an acceptable range and whether the VDC hit pattern was satisfactory. A VDC-wire hit analysis revealed that the number of wires, n_w , which fire should range between 5 and 8. Studies of the VDC intrinsic efficiency made using the deuteron elastic scattering data have shown, however, that the efficiency is optimal when this condition is relaxed to $3 < n_w < 10$. This revised condition was therefore used in the final replay of all the data.

The integral-time-spectrum method [22] involving the use of a lookup table was used to convert drift times associated with each accepted event to drift distances. These drift times and corresponding wire numbers were used to determine the position where the helion and deuteron trajectories, respectively, intersect the focal plane. This was done by least squares fitting a linear function to points which have wire number and drift distance, respectively, as coordinates.

Because of the trigger logic used in the ($d, ^3\text{He}$) mode, the signal-to-noise ratios in the spectra were still rather low. Two additional software cuts were therefore implemented during the analysis of pickup data. This involved the setting of gates on spectra in which pulse heights for paddle 1 associated with the left and right photomultiplier tubes, respectively,

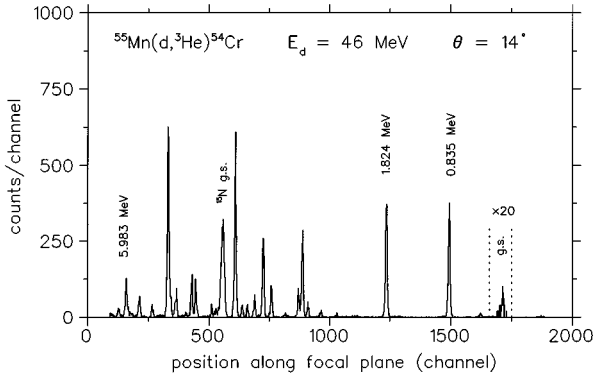


FIG. 2. A focal-plane position spectrum associated with the $^{55}\text{Mn}(d,^3\text{He})^{54}\text{Cr}$ reaction obtained at a spectrometer angle of 14° . The $^{15}\text{N}(\text{g.s.})$ peak is due to $(d,^3\text{He})$ reactions on the oxygen nuclei present in the Mylar target backing used.

were plotted against the focal-plane position. A typical focal-plane position spectrum generated from helion data is shown in Fig. 2. Since paddle 1 was operated in coincidence with paddle 2 when acquiring the elastic scattering data, the signal-to-noise ratio in focal-plane spectra was excellent, thereby obviating the need for the two cuts discussed above. A typical focal-plane position spectrum generated from (d,d) -mode data is shown in Fig. 3.

All peaks appearing in focal-plane position spectra generated from pickup data were fitted using the peak-fitting program FIT2.1 [23] assuming Gaussian line shapes. An initial fit was done to the resolved peaks in each spectrum to obtain an average FWHM. The spectra were then refitted with the peak widths fixed to the average FWHM value, allowing the intensities and centroids of the resolved and closely spaced peaks to be extracted.

For each pickup data set a momentum calibration of the focal plane was established using the centroids of five to six prominent (counts > 60) peaks corresponding to known ^{54}Cr final states in conjunction with knowledge of the measured beam energy and spectrometer angle. Standard nonrelativistic kinematics [24,25] were used to calculate the ejection

momenta. Following an F -test analysis of reduced chi-squared values in which a quadratic function was found to optimally parametrize the dependence of the focal-plane position on helion momenta, a quadratic linear least squares fit was used to obtain the momentum calibration of the focal plane. This momentum calibration in conjunction with the peak centroids was used to calculate the excitation energies E^* of the final states observed. The total uncertainty associated with these energies was determined by combining in quadrature the uncertainties associated with the momentum calibration and peak centroids, respectively. This uncertainty ranged from 1 to 13 keV (see Table III).

In the nonrelativistic approximation the relationship between the momentum resolving power, $\Delta P/P$, the particle energy E , and energy resolution ΔE is given by

$$\frac{\Delta E}{E} = \frac{2\Delta P}{P}. \quad (1)$$

The energy resolution for each run was calculated from Eq. (1) using the momentum calibration and the FWHM of resolved states, and was found to vary between 32 and 60 keV in the data analyzed. An average resolution of ~ 40 keV was obtained.

B. Angular distributions

Since the counting statistics associated with ^{54}Cr final states observed in spectra for angles $\theta \geq 30^\circ$ were rather poor, only pickup data acquired in the 6° – 30° angular range were used to extract spectroscopic factors. Pickup differential cross sections were calculated only for final states which were observed at the same excitation energy, to within statistical uncertainty, at more than six spectrometer angles. The excitation energies of the 24 ^{54}Cr states which were found to satisfy this criterion are tabulated in Table III. Only two of these states, observed at excitation energies of 5.574 MeV and 5.771 MeV, respectively, did not correspond to within statistical uncertainty with the adopted levels for ^{54}Cr [26,27].

The absolute center-of-mass (c.m.) differential cross section associated with the transition to the i th final state, reached via the $^{55}\text{Mn}(d,^3\text{He})^{54}\text{Cr}_i$ reaction, at an angle $\theta_{\text{c.m.}}$, was calculated using the formula

$$\frac{d\sigma}{d\Omega}(\theta_{\text{c.m.}}) = \frac{J_{\text{nr}} Y_i \cos(\theta/2)}{N_d \Delta \Omega n_i T_{k600} L \epsilon_V \epsilon_P}. \quad (2)$$

J_{nr} is the nonrelativistic Jacobian used to transform differential cross sections from the laboratory to the c.m. frame. The uncertainty in this factor, which was calculated using standard formulas [24], was found to be negligible.

The background in the focal-plane position spectra was assumed to be negligible in the determination of the yield Y_i associated with the transition to the i th final state. Two approaches were used to determine Y_i . In the case of well-resolved states, Y_i was determined by summing the counts in the peak of interest, while for unresolved states a Gaussian peak-fitting procedure, again using the program FIT2.1, was used to determine the yields. In the former case the uncertainty associated with Y_i was taken to be $\sqrt{Y_i}$, while in the

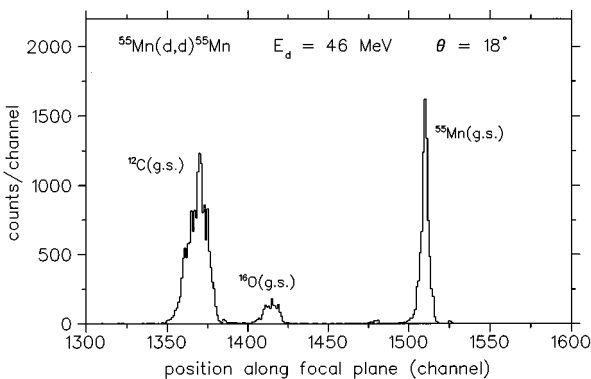


FIG. 3. A focal-plane position spectrum associated with the $^{55}\text{Mn}(d,d)^{55}\text{Mn}$ reaction obtained at a spectrometer angle of 18° . The $^{16}\text{O}(\text{g.s.})$ and $^{12}\text{C}(\text{g.s.})$ peaks are due to (d,d) reactions on the oxygen and carbon nuclei present in the Mylar target backing used.

latter case the corresponding uncertainty was obtained from the program MINUIT [28], which FIT2.1 calls to do the function minimization. The uncertainty (1σ) associated with yields stemming from the setting of software gates mentioned above was estimated to be $\leq 2\%$.

The $\cos(\theta/2)$ term in Eq. (2) is included because the target angle was always set to half the spectrometer angle in order to fix the target transformation factor to a value of 1.0.

N_d , the number of deuterons incident on the target, was obtained from the measured accumulated beam charge. It was electronically corrected for the fractional live time of the data acquisition system, L , which was monitored as described in Sec. II. The uncertainty in the measured accumulated charge was $\leq 1\%$.

The solid angle $\Delta\Omega$ subtended by the entrance collimator to the spectrometer for the geometry used was 1.34 msr. The uncertainty in $\Delta\Omega$, calculated by propagating the experimentally measured uncertainties in the collimator radius, length, and the target-collimator distance in the normal manner, was $< 1\%$. The uncertainty in $\Delta\Omega$ due to the beam spot size was negligible.

The number of ⁵⁵Mn nuclei per unit target surface area, n_t , was calculated from the measured thickness of the ⁵⁵Mn layer deposited onto the Mylar backing by making use of the same ⁵⁵Mn density used by RUMP to calculate thicknesses from the RBS spectra (see Sec. II). As discussed in Sec. II the uncertainty in n_t was estimated to be 5% (1σ).

The transmission efficiency of the $k = 600$ spectrometer, T_{k600} , was investigated using a variable slot collimator. It was found that 100% transmission occurred when using a slot located at ± 27.5 mm in both vertical and horizontal directions from the center of this collimator. In view of the collimator geometry used in this study, T_{k600} was therefore taken to be 100%.

The total VDC detection efficiency ϵ_V for helions is the product of its geometric and intrinsic efficiencies. The relative VDC geometric efficiency was checked by sweeping the helion peak associated with the excitation of the first excited state of ⁵⁴Cr, across the focal plane, by adjusting the spectrometer magnetic fields. It was found to be 100% to within statistics. The intrinsic efficiency was obtained by studying the VDC hit patterns for deuteron elastic scattering data. An average efficiency of 99% was obtained. The former efficiency was determined relative to the paddle efficiency ϵ_P , which was assumed to be 100%.

The average uncertainties associated with the pickup differential cross sections due to counting statistics ranged between 24% (for the weakest transition to the ⁵⁴Cr ground state) and 3% (for the transition to the state observed at 3.788 MeV excitation) while the combined uncertainty (1σ) associated with the target thickness, current integration, solid angle, and setting of software gates was estimated to be 6%. Absolute differential cross sections for the ⁵⁵Mn(d,d)-⁵⁵Mn(g.s.) reaction at $E_d=46$ MeV were calculated using an expression similar in form to Eq. (2). The deuteron yield was obtained by summing the counts in the ⁵⁵Mn ground state peak since the background in focal-plane spectra was negligible when acquiring elastic scattering data. The uncertainties associated with the (d,d) cross sections due to counting statistics were $\leq 4\%$ while the combined uncertainty (1σ) associated with the target thickness, current

integration, and solid angle was estimated to be 5%. Figure 4 shows the c.m. elastic scattering angular distribution obtained while measured c.m. angular distributions associated with transitions to the 24 ⁵⁴Cr final states observed are plotted in Figs. 5–11. Only the uncertainties contributing to random scatter obtained by combining in quadrature the uncertainty due to counting statistics and the estimated uncertainty (1σ) in target thickness are shown in these figures. The latter component was included since two targets were used to measure the angular distributions.

C. DWBA analyses

Pickup spectroscopic factors C^2S_{ijl} are associated with the transfer of a proton having orbital and total angular momentum l and j , respectively, in the ⁵⁵Mn($d,^3$ He)-⁵⁴Cr_{*i*} reaction, leading to the *i*th final state of ⁵⁴Cr. These were determined by normalizing a distorted-wave Born approximation (DWBA) angular distribution to the measured angular distribution. The normalization was done by minimizing χ^2 , defined by

$$\chi^2 = \sum_{\theta_{c.m.}} \left(\frac{\sigma_{\text{expt}}(\theta_{c.m.})_i - C^2S_{ijl}\sigma_{\text{DWBA}}(\theta_{c.m.})_{ijl}}{\Delta\sigma_{\text{expt}}(\theta_{c.m.})_i} \right)^2, \quad (3)$$

where $\sigma_{\text{expt}}(\theta_{c.m.})_i$ is the experimentally measured c.m. differential cross section associated with the transition to the *i*th final state, $\Delta\sigma_{\text{expt}}(\theta_{c.m.})_i$ is the uncertainty [obtained by combining in quadrature the uncertainty due to counting statistics and estimated uncertainty (1σ) in target thickness] associated with this cross section, and $\sigma_{\text{DWBA}}(\theta_{c.m.})_{ijl}$ is the corresponding DWBA differential cross section.

DWBA differential cross sections were calculated with the computer code DWUCK4 [29] using a local, zero-range formalism. Nonlocal and finite-range corrections [30] were not applied since in the first instance we are interested in relative spectroscopic factors which have been shown to be insensitive to the inclusion or omission of these corrections

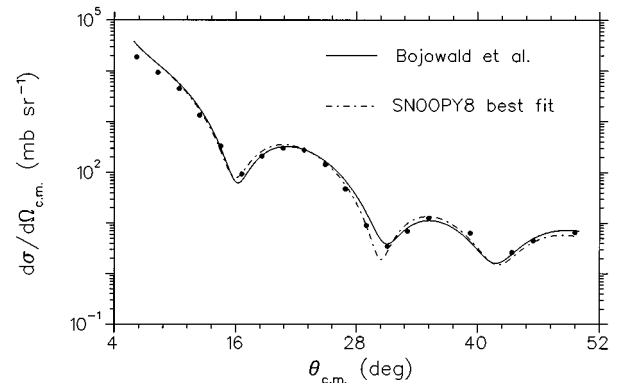


FIG. 4. Measured c.m. angular distribution for the ⁵⁵Mn(d,d)-⁵⁵Mn(g.s.) reaction at an incident energy of 46 MeV. If not shown the uncertainty (see text) in differential cross section is smaller than the size of the plotting symbol. The solid curve is a prediction based on the global parametrization by Bojowald *et al.* [13], while the dashed line is a prediction based on a potential having the same form as that of Bojowald *et al.*, but with parameters optimized using the code SNOOPY8 [32].

TABLE II. Optical-model potential parameters used in the DWBA analysis of angular distributions associated with the $^{55}\text{Mn}(d, ^3\text{He})^{54}\text{Cr}$ reaction at an incident energy of 46 MeV.

Channel	V (MeV)	r_v (fm)	a_v (fm)	W_{vol} (MeV)	$4W_{\text{surf}}$ (MeV)	r_w (fm)	a_w (fm)	$V_{l.s}$ (MeV)	$r_{l.s}$ (fm)	$a_{l.s}$ (fm)	r_c (fm)
$^{55}\text{Mn} + d$	82.14	1.18	0.79	0.08	53.00	1.27	0.84	4.73	0.92	0.61	1.30
$^{54}\text{Cr} + ^3\text{He}$	171.63	1.14	0.71	19.07		1.60	0.88				1.40
Proton	a	1.21	0.65					$\lambda=25$	1.21	0.65	1.30

^aWell depth was adjusted by the program DWUCK4 [29] to reproduce the experimental proton separation energies.

[2,31]. In the case of the $(d, ^3\text{He})$ reaction, DWBA differential cross sections are related to the corresponding DWUCK4 cross sections via the relation

$$\sigma_{\text{DWBA}}(\theta_{\text{c.m.}}) = \frac{N_0}{2j+1} \sigma_{\text{DWUCK4}}(\theta_{\text{c.m.}}), \quad (4)$$

where j is the total angular momentum transfer and N_0 is the Bassel normalization factor which is equal to 2.95 in the case of the $(d, ^3\text{He})$ reaction [29].

Part of the input needed by DWUCK4 to calculate σ_{DWBA} is a specification of the potentials needed to generate the distorted waves for the entrance and exit channels, and to calculate the bound-state wave functions. An optical-model (OM) potential having a form identical to the one used by Bojowald *et al.* to obtain a global OM potential for deuteron scattering up to 100 MeV [13] was used to obtain the distorted-wave functions for the $d + ^{55}\text{Mn}$ channel. This potential, which comprised Coulomb, central, imaginary volume, imaginary surface, and real spin-orbit terms, had the form

$$U(r) = V_c(r) - Vf_v(r, R_v, a_v) - i \left[W_{\text{vol}} f_w(r, R_w, a_w) - 4a_w W_{\text{surf}} \frac{d}{dr} f_w(r, R_w, a_w) \right] + V_{l.s} \left(\frac{\hbar}{m\pi c} \right)^2 (\mathbf{l} \cdot \mathbf{s}) \frac{1}{r} \frac{d}{dr} f_{l.s}(r, R_{l.s}, a_{l.s}), \quad (5)$$

where

$$f_k = \left[1 + \exp\left(\frac{r - R_k}{a_k}\right) \right]^{-1}$$

and

$$R_k = r_k A^{1/3}.$$

The values of the parameters used in conjunction with the potential form above are given in Table II. These parameters were obtained from an analysis of the angular distribution associated with the $^{55}\text{Mn}(d, d)^{55}\text{Mn}(\text{g.s.})$ ($E_d = 46$ MeV, $6^\circ \leq \theta \leq 48^\circ$) reaction. This analysis was performed using the computer code SNOOPY8 [32] which utilizes a chi-square minimization procedure to obtain best-fit OM potential parameters, by minimizing a quantity χ^2 , defined as

$$\chi^2 = \sum_{\theta_{\text{c.m.}}} \left(\frac{\sigma_{\text{expt}}(\theta_{\text{c.m.}}) - \sigma_{\text{theor}}(\theta_{\text{c.m.}})}{\Delta\sigma_{\text{expt}}(\theta_{\text{c.m.}})} \right)^2, \quad (6)$$

where $\sigma_{\text{expt}}(\theta_{\text{c.m.}})$ is the measured c.m. elastic scattering differential cross section, $\Delta\sigma_{\text{expt}}(\theta_{\text{c.m.}})$ is the uncertainty associated with this cross section, and $\sigma_{\text{theor}}(\theta_{\text{c.m.}})$ is the corresponding differential cross section calculated by SNOOPY8. Initial values of the potential parameters used in the minimization procedure were obtained from the parametrization of Bojowald *et al.* The potential parameters which yielded the lowest χ^2 are shown in Table II, while the elastic angular distribution calculated using these parameters is shown in Fig. 4.

Bound-state potential parameters, especially the radius parameter, strongly affect the magnitude of spectroscopic factors. In this study, a 1% change in the bound-state potential radius was found to cause a 7% change in absolute spectroscopic factors but negligible change in relative spectroscopic factors. A standard bound-state potential comprising a Coulomb, central, and Thomas spin-orbit term with $\lambda = 25$ was used. Standard values $a_v = a_{l.s} = 0.650$ fm were used. The potential well depth was automatically adjusted by DWUCK4 to reproduce the experimental proton separation energies. The bound-state potential radii ($R_v = R_{l.s}$) were adjusted in order to obtain an fp shell proton occupancy of ~ 5 in ^{55}Mn . The bound-state potential parameters used are shown in Table II.

Since helion beams are not available at NAC, an optical potential and the corresponding distorted wave functions for the exit channel could not be determined from the analysis of measured helion elastic scattering data. Instead ^3He optical potentials found in the literature were used. Trost *et al.* studied the mass dependence of the helion optical potential for light to medium weight nuclei at a beam energy of 41 MeV [12]. They employed a ‘‘physical’’ potential characterized by a volume integral of the real part $J_R(^{58}\text{Ni}) = 330$ MeV fm³. This potential has the same form as that given by Eq. (5), but with W_{vol} and $V_{l.s}$ set to zero. The other study of ^3He optical potentials was by Barr and DelVecchio [11] who studied ^3He elastic scattering data at 39.7 MeV on targets ranging from ^{12}C to ^{197}Au . The optical potentials they studied had a form similar to the one in Eq. (5), but with W_{surf} and $V_{l.s}$ set to zero.

Since the $6^+ ^{54}\text{Cr}$ final state observed at 3.220 MeV excitation can only be reached via $0f_{7/2}$ transfer, the angular distribution associated with this state was used to assess the relative merits of the potential parametrizations of Trost *et al.* and Barr and DelVecchio. DWBA angular distributions

TABLE III. Spectroscopic information from the ⁵⁵Mn(*d*,³He)⁵⁴Cr reaction at an incident energy of 46 MeV. New spin assignments shown have been made as discussed in the text.

From Ref. [27]			Present work				New $J'\pi$ assignment		
E^* (MeV)	ΔE^* (keV)	$J'\pi$	E^* (MeV)	ΔE^* (keV)	C^2S				
					$\ell=0$	$\ell=1$	$\ell=2$	$\ell=3$	
0.0		0 ⁺	0.0	0				0.02	
0.835	≤1	2 ⁺	0.835	1				0.85	
1.824	≤1	4 ⁺	1.824	2				0.99	
2.620	≤1	2 ⁺	2.622	4		0.01		0.02	
3.074	≤1	2 ⁺	3.076	3		0.05		0.09	
3.160	≤1	4 ⁺	3.159	1		0.09		0.84	
3.222	≤1	(6) ⁺	3.220	5				0.27	6 ⁺
3.437	≤1	2 ⁺	3.429	8		0.01		0.05	
3.655	≤1	4 ⁺	3.656	4				0.34	
3.786	≤1	(4,5) ⁺	3.788	3				1.06	5 ⁺
3.928	≤1	2 ⁺	3.926	4		0.05		0.22	
4.042	≤1	(7) ⁺	4.041	4				0.13	6 ⁺
4.127	≤1	3 ⁻	4.128	5	0.04		0.07		
4.245	5	2 ⁺ ,3 ⁻	4.237	4	0.61		0.35		3 ⁻
4.561	11		4.551	6	0.02		0.11		(1-4) ⁻
4.618	6		4.619	4	0.02		0.11		(1-4) ⁻
4.865	4	(1 ⁻ ,4 ⁺)	4.868	7		0.03	0.67		
4.936	6		4.936	8	0.05		0.87		(1-4) ⁻
5.189	≤1	(0,1,2)	5.191	11	0.04		0.47		(1,2) ⁻
5.321	10		5.310	9	0.96				(2-3) ⁻
			5.574	10	0.02		0.33		(1-4) ⁻
			5.771	12	0.05		0.34		(1-4) ⁻
5.981	10		5.983	13	0.12		0.59		(2,3) ⁻
6.113	10		6.104	6	0.02		0.22		(1-4) ⁻

associated with the transition were obtained using these parametrizations along with the OM entrance channel and bound-state potential parameters shown in Table II. Two resulting fits to the experimental data are shown in Fig. 5. The parametrization labeled ‘‘FIT G’’ used by Barr and DelVecchio was found to be the most suitable, as it resulted in a better fit to experimental points at forward angles which are more important for determining spectroscopic factors. The corresponding parameter values used are shown in Table II.

For ⁵⁵Mn it was assumed that proton pickup from the 0*f*_{7/2}, 0*f*_{5/2}, 1*p*_{3/2}, 1*p*_{1/2}, 0*d*_{5/2}, 0*d*_{3/2}, and 1*s*_{1/2} subshells was possible. Since ⁵⁵Mn has a known ground-state spin and parity of $\frac{5}{2}^-$, it is possible to establish the range of ⁵⁴Cr final state spins and parities for proton pickup from these subshells. This was done using the relation between parities

$$\pi_{\text{final}} = \pi_{\text{initial}} \pi_{\text{transfer}} \quad (7)$$

and the triangular inequality

$$|J_i - j| \leq J' \leq J_i + j, \quad (8)$$

where J' is final state spin, J_i the ground-state spin, and j the spin transfer. Since for a given ℓ transfer DWBA angular distributions are insensitive to the j transfer [33], it was not possible to uniquely determine the j transfer by fitting the calculated angular distribution to the experimental data. In-

stead it was further assumed that an $\ell=1$ transfer implied 1*p*_{3/2} proton transfer for $1 \leq J' \leq 4$, an $\ell=2$ transfer implied 0*d*_{3/2} proton transfer for $1 \leq J' \leq 4$, and an $\ell=3$ transfer implied 0*f*_{7/2} proton transfer for $1 \leq J' \leq 6$.

Mixed transitions involving at most two types of (j, ℓ) transfer, say, (j_a, ℓ_a) and (j_b, ℓ_b), were considered possible. Spectroscopic factors associated with each transfer were extracted using Eq. (3) with the expression for $C^2S\sigma_{\text{DWBA}}$ now reading

$$C^2S_{a+b}\sigma_{\text{DWBA}}(\theta_{\text{c.m.}}) = 2.95C^2S_{a+b} \left(\frac{\gamma}{2j_a+1} \sigma_{\text{DWUCK4}}(\theta_{\text{c.m.}})_{j_a l_a} + \frac{(1-\gamma)}{2j_b+1} \sigma_{\text{DWUCK4}}(\theta_{\text{c.m.}})_{j_b l_b} \right), \quad (9)$$

where $0 \leq \gamma \leq 1$. Spectroscopic factors associated with (j_a, ℓ_a) and (j_b, ℓ_b) transfers to the same final state are thus given by

$$C^2S_{j_a l_a}(\theta_{\text{c.m.}}) = \gamma C^2S_{a+b}(\theta_{\text{c.m.}}) \quad (10)$$

and

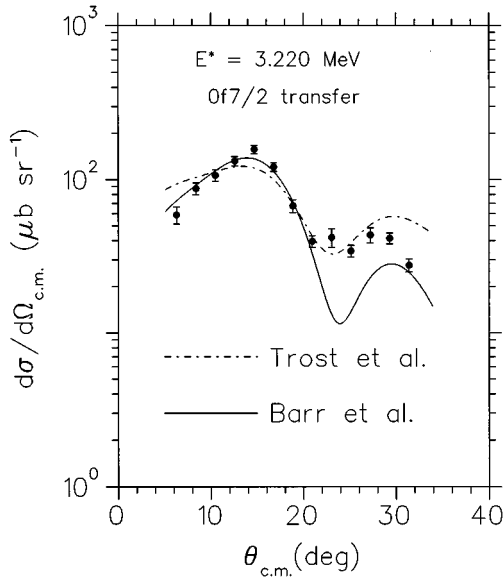


FIG. 5. Measured c.m. angular distribution associated with the $^{55}\text{Mn}(d, ^3\text{He})^{54}\text{Cr}(E^* = 3.220 \text{ MeV})$ reaction at an incident energy of 46 MeV. The curves result from DWBA calculations made using the descriptions of Barr and DeVecchio [11] and Trost *et al.* [12] for the exit channel potential, respectively. The optical model potential parameters used to calculate the entrance channel and bound-state wave functions are shown in Table II.

$$C^2S_{j_b l_b}(\theta_{\text{c.m.}}) = (1 - \gamma)C^2S_{a+b}(\theta_{\text{c.m.}}). \quad (11)$$

Fits to each pickup angular distribution measured were made using the corresponding DWBA angular distribution associated with $\ell = 0, 1, 2,$ or 3 transfer. Those angular distributions which were not well fitted with one ℓ transfer were refitted, allowing for mixed transitions involving any two of $\ell = 0, 1, 2,$ or 3 transfers. By finding the ℓ transfer(s) which yielded the lowest χ^2 the (j, l) transfer(s) associated with that transition could be ascertained. In the final analysis spectroscopic factors associated with measured angular distributions which displayed an $\ell = 3$ transfer signature were calculated by restricting the angular range in Eq. (3) to the forward angles, $\theta_{\text{c.m.}} \leq 20^\circ$, where the cross section peaks.

The best fits of the calculated angular distributions to the corresponding measured data are shown in Figs. 6–11, while the spectroscopic factors extracted via these fits are shown in Table III. We stress here that the pickup normalization was arbitrarily adjusted as described above in order to reproduce the simple shell-model result of five protons residing in the fp shell. Because of the weighting used in Eq. (3), the uncertainties in the extracted spectroscopic factors stemming from the uncertainties in experimental cross section ranged between 16% and 6% for the transitions to the ground and 3.788 MeV states of ^{54}Cr , respectively.

All $\ell = 3$ strength was found to be localized to an excitation region below 4.1 MeV in ^{54}Cr . A relatively small strength of 0.02 was found for the transition to the ^{54}Cr 0^+ ground state which can only be reached by $0f_{5/2}$ transfer, while the other 0^+ adopted levels at 2.830 and 4.013 MeV

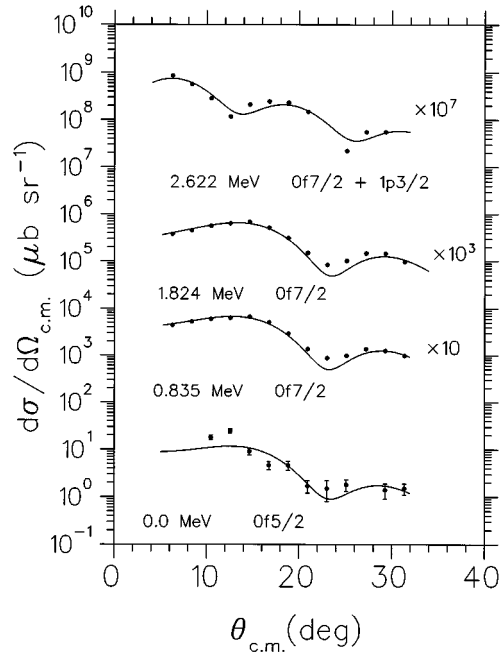


FIG. 6. Measured c.m. angular distributions associated with the $^{55}\text{Mn}(d, ^3\text{He})^{54}\text{Cr}$ reaction at an incident energy of 46 MeV for final state excitation energies ranging between 0.0 and 2.622 MeV. If not shown the uncertainty (see text) in differential cross section is smaller than the size of the plotting symbol. The curves result from DWBA calculations made using the potential parameters shown in Table II and assuming (j, l) transfer(s) as indicated.

were not seen. These observations support the expectation that the $0f_{5/2}$ proton orbital is essentially empty in ^{55}Mn . Further support for this comes from shell-model calculations as discussed in Sec. IV B. Any remaining $\ell = 3$ strength was

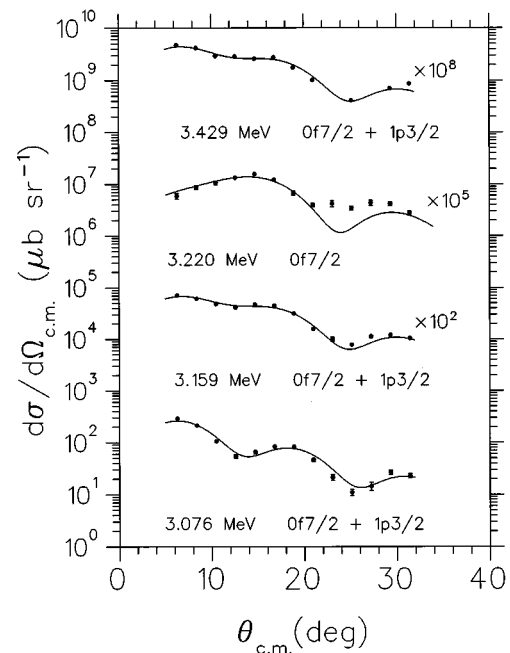


FIG. 7. The same as in Fig. 6 but for ^{54}Cr final state excitation energies ranging between 3.076 and 3.429 MeV.

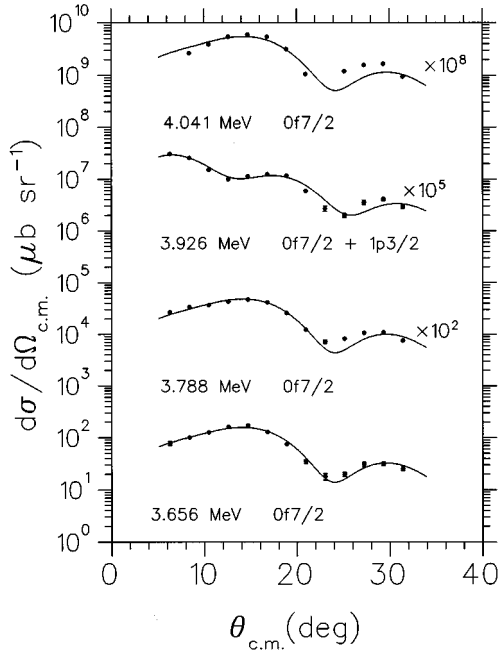


FIG. 8. The same as in Fig. 6 but for ⁵⁴Cr final state excitation energies ranging between 3.656 and 4.041 MeV.

therefore assumed to be associated with 0f_{7/2} transfer.

Pickup from the 1s0d shell was also observed, leading to final states beginning with the known 3⁻ state at an excitation energy of 4.127 MeV. For all such states the best fits to the angular distributions were obtained using a mixture of ℓ = 0 (*j* = 1/2) and ℓ = 2 (assumed *j* = 3/2) pickup. However, wherever the ℓ = 0 spectroscopic factor was less than 0.05 the improvement over pure ℓ = 2 was marginal, and we feel it prudent not to assign *J*' = (2,3)⁻ to these states on the

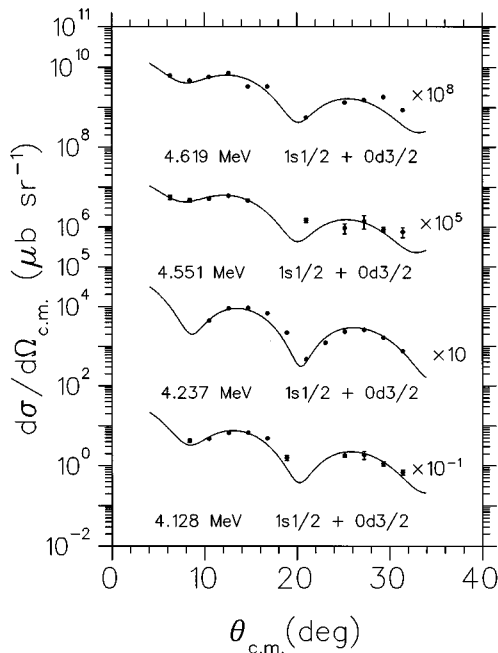


FIG. 9. The same as in Fig. 6 but for ⁵⁴Cr final state excitation energies ranging between 4.128 and 4.619 MeV.

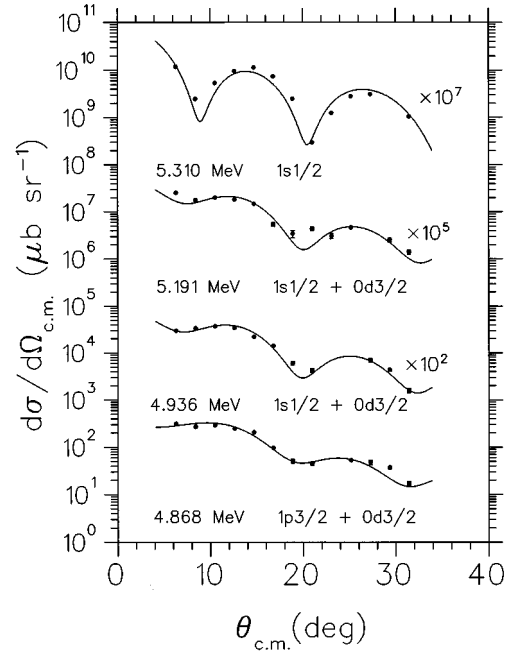


FIG. 10. The same as in Fig. 6 but for ⁵⁴Cr final state excitation energies ranging between 4.868 and 5.310 MeV.

basis of such small ℓ = 0 contributions. We have thus assigned *J*' = (1-4)⁻ to these states in Table III. However, for the adopted levels at 4.245, 5.321, and 5.981 MeV the ℓ = 0 contribution to the pickup cross section is much more secure, allowing us to assign *J*' = (2,3)⁻ to these states and, hence, *J*' = 3⁻ to the 4.245 MeV state using prior information. Also, the spin assignment of *J*' = (0,1,2) to the adopted level at 5.189 MeV can be tightened to (1,2)⁻.

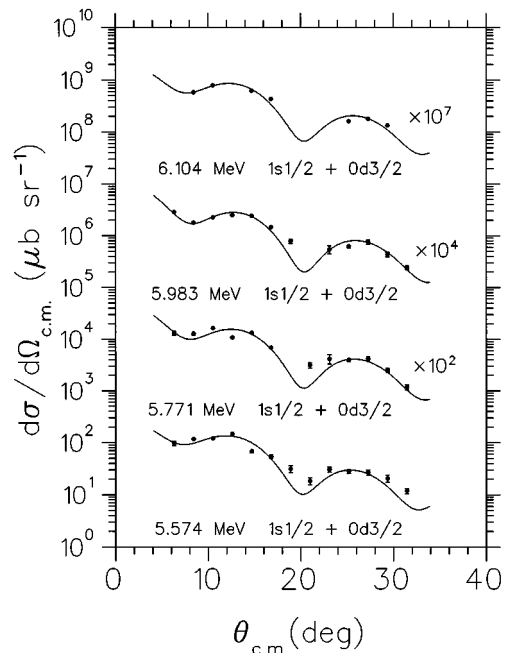


FIG. 11. The same as in Fig. 6 but for ⁵⁴Cr final state excitation energies ranging between 5.574 and 6.104 MeV.

TABLE IV. Calculated stripping strengths associated with transitions to positive parity states reached via the $^{55}\text{Mn}(\alpha,t)^{56}\text{Fe}$ reaction. Results were obtained from a shell-model calculation using a new effective interaction for $A = 41\text{--}66$ nuclei [14]. Shown are only those final states for which the spectroscopic strength associated with any ℓ transfer is ≥ 0.02 .

J'_k	E^* (MeV)	$\frac{[J']}{[J_i]} C^2S$			
		$0f_{7/2}$ $\ell=3$	$1p_{3/2}$ $\ell=1$	$0f_{5/2}$ $\ell=3$	$1p_{1/2}$ $\ell=1$
2 ₁	0.888	1.400	0.003	0.002	
4 ₁	2.107	0.215			
2 ₂	2.567	0.237	0.003	0.001	
2 ₃	3.148	0.033	0.007	0.002	0.002
4 ₂	3.162	0.071	0.011		
1 ₁	3.197	0.175	0.004		
3 ₁	3.316	0.016	0.002		
6 ₁	3.458	0.714			
2 ₄	3.527	0.004	0.091	0.007	0.025
3 ₂	3.585	0.041	0.004		
2 ₅	3.675		0.154	0.007	0.042
6 ₂	3.737	0.310			
3 ₃	4.044	0.001	0.173	0.006	0.062
4 ₃	4.176		0.030		
3 ₄	4.421	0.004	0.006	0.004	0.016
4 ₄	4.480		0.026	0.005	
3 ₅	4.608	0.007	0.450	0.036	0.099
6 ₃	4.614	0.076			
2 ₆	4.663	0.017	0.002	0.005	0.016
4 ₅	4.668	0.003	0.021		
3 ₆	4.814	0.002	0.090	0.011	0.007
1 ₂	4.903	0.037	0.158	0.001	
5 ₁	4.969			0.018	
1 ₃	5.042	0.006	0.034		
4 ₆	5.042	0.008	0.242	0.078	
5 ₂	5.061			0.016	
3 ₇	5.100	0.002	0.027	0.001	
1 ₄	5.400		0.034	0.003	

The observed adopted level at 4.865 MeV has a spin assignment of $(1^-, 4^+)$. An optimal fit to the corresponding angular distribution was obtained by allowing for ℓ transfers of 1 and 2, and it is likely that the state observed is a doublet. No new information about the spin assignment for this level was therefore obtained.

As mentioned in Sec. III B, two new levels were observed at excitation energies of 5.574 and 5.771 MeV, respectively. Their associated angular distributions were fitted well by allowing for $\ell = 0, 2$ transfer, and we again assign $J' = (1-4)^-$ to these states.

All new spin assignments made on the basis of the DWBA analyses, as discussed above, are shown in the last column of Table III. The spin assignments of $6^+, 5^+$, and 6^+ made to states at observed excitation energies of 3.220, 3.788, and 4.041 MeV, respectively, will be discussed in Sec. IV together with the results of shell-model calculations and NEWSR analyses of $0f_{7/2}$ pickup and stripping transfer strength.

TABLE V. Calculated pickup strengths associated with transitions to positive parity states reached via the $^{55}\text{Mn}(d, ^3\text{He})^{54}\text{Cr}$ reaction. Results were obtained from a shell-model calculation using a new effective interaction for $A = 41\text{--}66$ nuclei [14]. Shown are only those final states for which the spectroscopic strength associated with any ℓ transfer is ≥ 0.02 .

J'_k	E^* (MeV)	C^2S			
		$0f_{7/2}$ $\ell=3$	$1p_{3/2}$ $\ell=1$	$0f_{5/2}$ $\ell=3$	$1p_{1/2}$ $\ell=1$
2 ₁	0.911	0.804	0.004	0.002	
4 ₁	1.902	1.186	0.002		
2 ₂	2.352	0.130	0.015		0.001
2 ₃	2.799	0.034	0.005		
4 ₂	2.808	1.096	0.021	0.001	
4 ₃	2.996	0.016	0.003	0.001	
6 ₁	3.049	0.278			
3 ₁	3.230	0.151	0.006		
3 ₂	3.438	0.046	0.001		
5 ₁	3.521	1.075		0.001	
4 ₄	3.602	0.050		0.001	
6 ₂	3.754	0.159			
4 ₅	4.278	0.087	0.001		
3 ₃	4.557	0.018	0.003		
5 ₂	4.701	0.034			
3 ₄	4.738	0.015			
6 ₃	4.990	0.026			

IV. SHELL-MODEL CALCULATIONS AND SUM-RULE ANALYSES

A. Shell-model calculations

The shell-model calculations assume an inert ^{40}Ca core and a model space consisting of

$$0f_{7/2}^n (1p_{3/2} 0f_{5/2} 1p_{1/2})^m + 0f_{7/2}^{n-1} (1p_{3/2} 0f_{5/2} 1p_{1/2})^{m+1}$$

configurations, with $n+m$ the number of valence nucleons for a given nucleus, and n the maximum number of nucleons allowed in the $0f_{7/2}$ orbit by the Pauli principle. Matrix elements of the effective interaction were fixed by the requirement of a best fit between experiment and theory for a large set of energy levels in $A = 41\text{--}66$ nuclei [14]. Calculated spectroscopic factors associated with transitions to ^{56}Fe and ^{54}Cr final states reached via the $^{55}\text{Mn}(\alpha,t)^{56}\text{Fe}$ and $^{55}\text{Mn}(d, ^3\text{He})^{54}\text{Cr}$ reactions are shown in Tables IV and V, respectively. No significant $0f_{7/2}$ stripping strength is predicted to lie above 3.737 MeV. This is in good agreement with Matoba's results (see Table I) which show the last fragment of $0f_{7/2}$ strength to be located at 3.78 MeV. The shell-model results also show negligible $0f_{5/2}$ and $1p_{1/2}$ pickup strength, thus supporting the assumption made in the DWBA analyses that $\ell = 3$ transfer implies $0f_{7/2}$ transfer and that an $\ell = 1$ transfer implies $1p_{3/2}$ transfer.

B. Sum-rule analyses

Here we concentrate on the $0f_{7/2}$ transfer strength. The establishment of stripping and pickup spin distributions of this strength is first discussed.

For the stripping strength a summary of the spectroscopic information from Matoba's study [4] is given in Table I, together with the most recent adopted levels ($E^* \leq 4.0$ MeV) [5,6]. Except for the transition to the ^{56}Fe ground state (0^+), it was assumed that the $\ell=3$ strength seen by Matoba is associated with $0f_{7/2}$ proton transfer. The negligible $0f_{5/2}$ strength below 4.0 MeV excitation predicted by the shell model (see Table IV) supports this assumption.

The ^{56}Fe excited states at excitation energies of 0.85, 2.09, and 2.66 MeV as reported by Matoba correspond unambiguously with the adopted levels at 0.847, 2.085, and 2.658 MeV, respectively. These three states have spins of 2^+ , 4^+ , and 2^+ , respectively.

The mapping of the next three states reported by Matoba to the presently adopted ^{56}Fe levels is ambiguous because of a relatively large uncertainty of 40 keV associated with the excitation energies of these states. Matoba found an $\ell=3$ stripping strength of 0.08 to be associated with the complex state at $(2.97 + 3.15)$ MeV. By considering only excitation energies, this strength could be associated with transitions to adopted levels at energies of 2.942 ($J' = 0^+$), 2.960 ($J' = 2^+$), 3.070 [$J' = (3^-)$], 3.120 [$J' = (1^+)$], or 3.123 ($J' = 4^+$) MeV. ^{55}Mn has a ground-state spin $\frac{5}{2}^-$, and if it is assumed that an $\ell=3$ transfer implies a transfer of a proton to the $0f_{7/2}$ subshell, the only possible transitions are to the 2.960, 3.120, and 3.123 MeV states. The small stripping strength of 0.08 was therefore shared equally amongst final state spins of 1^+ , 2^+ , and 4^+ .

The state seen by Matoba at 3.40 MeV could correspond to adopted levels at excitation energies of 3.370 MeV ($J' = 2^+$) or 3.388 MeV ($J' = 6^+$), with the latter being the one suggested by Matoba [4]. If it is assumed that this is a 2^+ state, a significant deterioration in the quality of NEWSR fits results. Furthermore, the shell-model results shown in Table IV indicate the presence of a strong transition to a 6^+ ^{56}Fe final state at an excitation energy of 3.458 MeV. It was therefore assumed that this state corresponds to the adopted level at 3.388 MeV. The spectroscopic strength of 0.90 was therefore associated with a 6^+ final state.

The state seen by Matoba at 3.78 MeV could correspond to adopted levels at excitation energies of 3.748 ($J' = 2^+$), 3.756 ($J' = 6^+$), or 3.760 ($J' = 2-6$) MeV. In view of this and the uncertainties in parity assignments to the 3.760 MeV state, the strength of 0.25 associated with Matoba's state at 3.78 MeV was shared equally between 2^+ and 6^+ final states.

For the pickup strength, and in particular the particle occupancy in ^{55}Mn of proton orbits other than the $0f_{7/2}$, Table III shows that the summed $1p$ strength observed in the $^{55}\text{Mn}(d, ^3\text{He})^{54}\text{Cr}$ reaction is 0.24. Further, the weak excitation of the ^{54}Cr ground state (0^+) in this reaction strongly suggests a similarly small $0f_{5/2}$ occupancy. These observations are in line with the shell-model findings that for ^{55}Mn the $1p_{3/2}$ proton occupancy is 0.06, and that the $1p_{1/2}$ and $0f_{5/2}$ proton occupancies are negligible. As shown in Table III, three ^{54}Cr final states observed which are reached via $\ell=3$ transfer have uncertain spin assignments.

An $\ell=3$ pickup strength of 0.13 was found for the transition to the ^{54}Cr state observed at 4.041 MeV. This state corresponds with the adopted level at 4.042 MeV which has

an uncertain spin assignment of 7^+ . However, the angular distribution for pickup to this state is unambiguously $\ell=3$, and the assumption that this corresponds to $0f_{7/2}$ pickup limits the spins of this state to $1^+ \leq J' \leq 6^+$. It is therefore unlikely that the 4.042 MeV state has a spin of 7^+ . Gamma decay selection rules favor a large value of the spin. The shell-model results shown in Table V indicate a 6^+ state at 3.754 MeV with a pickup strength of 0.16. In view of the above we make a spin assignment of 6^+ to the 4.042 MeV state.

The next uncertain spin assignment was the one associated with the state observed at an excitation energy of 3.788 MeV. This excitation energy is consistent with that of the adopted level at 3.786 MeV which has a $(4^+, 5^+)$ spin assignment. There is also a ^{54}Cr adopted level at 3.799 MeV ~ 13 keV away from the 3.786 MeV state which cannot be resolved experimentally. This level is known to have a spin of 4^+ , however, so that the pickup strength of 1.06 must be associated solely with final state spin of 4^+ or 5^+ . The shell-model calculations predict a significant fragment of strength (1.08) to be located in a 5^+ state at an excitation of 3.521 MeV. Also, unless it is assumed that the bulk of the experimentally observed strength is associated with a 5^+ final state, very poor fits to the NEWSR are obtained. We thus make a spin assignment of 5^+ to the adopted level state at 3.786 MeV, and assume that the 4^+ state at 3.799 MeV is not seen. The possibility that the 3.799 MeV state is seen but not resolved will be explored further below.

Finally the adopted level observed at 3.220 MeV in this study has an uncertain spin assignment of 6^+ . This level, which has an associated strength of 0.27, most likely corresponds to the shell-model level 6^+ state at 3.049 MeV which has an associated strength of 0.278. Changing this spin assignment would also result in a significant deterioration of the sum-rule fits.

All the spin assignments made to ^{56}Fe and ^{54}Cr final states, as discussed above, are tabulated in Table VI, and are compared with the corresponding results of the shell-model calculation in Figs. 12 and 13.

Figures 12(a) and 13(a) compare the experimental and shell-model distributions of the $0f_{7/2}$ proton spectroscopic strength as a function of final state excitation energy and spin, and Figs. 12(b) and 13(b) compare the corresponding summed strengths as a function of final state spin. The overall agreement is good, particularly in the latter case.

Finally we turn to a sum-rule analysis of the $0f_{7/2}$ proton stripping and pickup spin distributions, using a technique based on a symmetrical form of the NEWSR [1]. The basic quantities involved are the partial spectroscopic sums $S_{J'}^+$ and $S_{J'}^-$, associated with transitions to final states of spin J' given in Table VI, together with the corresponding errors $\Delta S_{J'}^+$ and $\Delta S_{J'}^-$. The latter are estimated assuming a common fractional error σ in the partial sums, so that

$$\Delta S_{J'}^+ = \sigma S_{J'}^+, \quad \Delta S_{J'}^- = \sigma S_{J'}^-, \quad (12)$$

where $\sigma = 0.10$ in the absence of further information [1,2]. For $J > 0$, we then construct the quantities

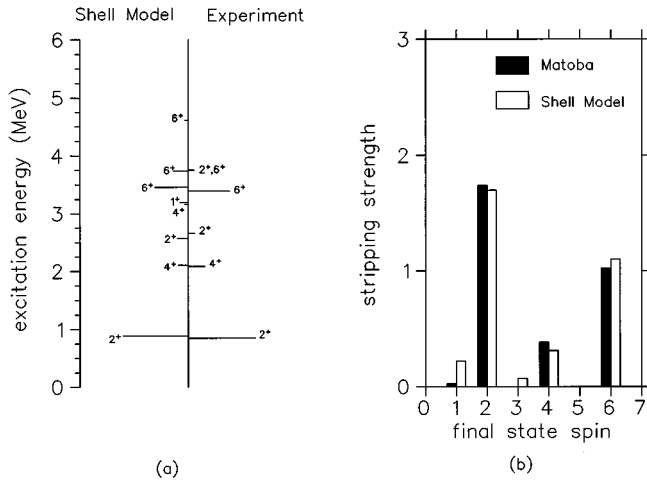


FIG. 12. Comparison of results from a recent $0f1p$ shell-model calculation with the $0f_{7/2}$ proton stripping spectroscopic strength shown in Table VI. In (a) spectroscopic strength is plotted as a function of ^{56}Fe excitation energy while the summed spectroscopic strength is plotted as a function of ^{56}Fe final state spin in (b). Shown are only those final states for which spectroscopic strength is > 0.05 .

$$Q_J = \sum_{J'} (-1)^{J_t + j + J'} \begin{Bmatrix} J & J_t & J_t \\ J' & j & j \end{Bmatrix} \{nS_{J'}^+ + (-1)^J S_{J'}^-\}, \quad (13)$$

where $J_t = \frac{5}{2}$ is the ^{55}Mn ground-state spin, $j = \frac{7}{2}$ is the

TABLE VI. Spectroscopic factors for $0f_{7/2}$ proton transfer on ^{55}Mn to reach final states of spin J' at excitation energy E^* in the final nucleus. The partial sums $S_{J'}^+$, $S_{J'}^-$, used in the text, are obtained by summing over final states of the same spin J' . The excitation energies of final states reached via stripping were obtained from Refs. [5,6] while those for pickup final states were obtained from this study.

J'	Stripping E^* (MeV)	$\frac{[J']}{[J_t]} C^2 S$	J'	Pickup E^* (MeV)	$C^2 S$
2 ⁺	0.847	1.45	2 ⁺	0.835	0.85
4 ⁺	2.085	0.36	4 ⁺	1.824	0.99
2 ⁺	2.658	0.14	2 ⁺	2.622	0.02
2 ⁺	2.960	0.027 ^a	2 ⁺	3.076	0.09
1 ⁺	3.120	0.027 ^a	4 ⁺	3.159	0.84
4 ⁺	3.123	0.027 ^a	6 ⁺ d	3.220	0.27
6 ⁺ b	3.388	0.90	2 ⁺	3.429	0.05
2 ⁺	3.748	0.125 ^c	4 ⁺	3.656	0.34
6 ⁺	3.756	0.125 ^c	5 ⁺ d	3.788	1.06
			2 ⁺	3.926	0.22
			6 ⁺ d	4.041	0.13

^aStrength of 0.08 distributed equally over final state spins of 1⁺, 2⁺, and 4⁺ as discussed in the text.

^bAssignment made on basis of Matoba's suggestion [4], sum-rule analyses, and shell-model calculations as discussed in the text.

^cStrength of 0.25 distributed equally over final state spins 2⁺ and 6⁺ as discussed in the text.

^dSpin assignments made as discussed in the text.

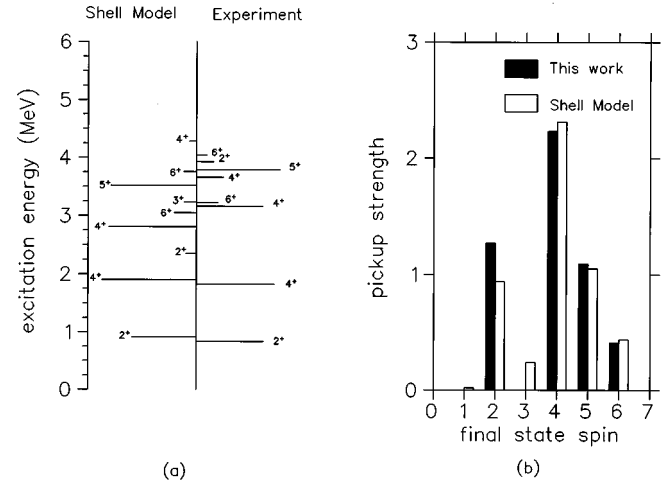


FIG. 13. Comparison of results from a recent $0f1p$ shell-model calculation with the $0f_{7/2}$ proton pickup spectroscopic strength shown in Table VI. In (a) spectroscopic strength is plotted as a function of ^{54}Cr excitation energy while the summed spectroscopic strength is plotted as a function of ^{54}Cr final state spin in (b). Shown are only those final states for which spectroscopic strength is > 0.05 .

transferred spin, n is a normalization constant [1] to be determined, and J is constrained by $0 \leq J \leq (N-1)$ where $N = \min\{[J_t], [j]\}$. For a perfect fit to the sum rules, a single value of n would result in $Q_J = 0$ for each of the N values of $J > 0$. However, the errors $\Delta S_{J'}^+$ and $\Delta S_{J'}^-$ of Eq. (12) propagate into errors ΔQ_J in the Q_J , so that

$$(\Delta Q_J)^2 = \sum_{J'} \left\{ \begin{Bmatrix} J & J_t & J_t \\ J' & j & j \end{Bmatrix} \right\}^2 \sigma^2 \{n^2 (S_{J'}^+)^2 + (S_{J'}^-)^2\}; \quad (14)$$

therefore, a standard form of the goodness of fit indicator, χ^2 , is given by

$$\chi^2 = \frac{1}{(N-2)} \sum_{J>0} \frac{Q_J^2}{(\Delta Q_J)^2}. \quad (15)$$

The fit can now be optimized by varying n , to determine the minimum value $\chi^2 = \chi_{\min}^2$, and the corresponding value of $n = n_{\min}$. The results are shown in Fig. 14. Closer inspection reveals that the sum rule for $J = 3$ is badly fitted, and is the principal cause of the rather large value of χ_{\min}^2 obtained for curve I in Fig. 14. Furthermore, the fit to this sum rule turns out to be particularly sensitive to a transfer of strength from the partial sum S_5^- to the partial sum S_4^- . Of course, other possibilities of reducing the original discrepancy exist, but a virtue of applying the sum rules is to focus attention on likely candidates. In the present case, the obvious focus is on S_4^- and S_5^- .

In this regard the possibility that the strong 5⁺ state seen at 3.788 MeV excitation in ^{54}Cr could be masking some strength to the 3.799 MeV (4⁺) state was investigated. This was done by attempting to deconvolute the yield which in the analysis above was assumed to be associated with the 3.786 MeV (4⁺, 5⁺) adopted level. Pickup data for which

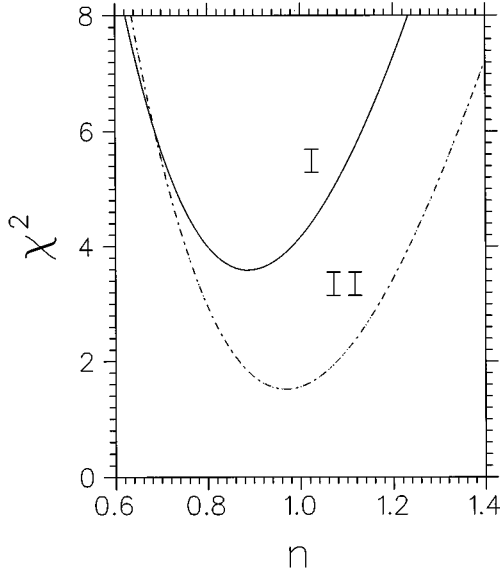


FIG. 14. Plot of goodness of fit indicator χ^2 versus normalization n . See text for discussion.

the average resolution was highest (32 keV FWHM) were used in the investigation. A single Gaussian function was first fitted to the region of interest in the ⁵⁴Cr spectrum. The Gaussian width was fixed to a mean width, determined from fits to resolved states in the vicinity of 3.786 MeV, while the peak centroid was fixed to that expected for the 3.786 MeV state. The resulting fit having an associated χ^2 per degree of freedom (ν) of 4.43 is shown in Fig. 15. Two Gaussians with centroids fixed at 3.786 and 3.799 MeV, and both widths fixed to the value used before, were then fitted to the

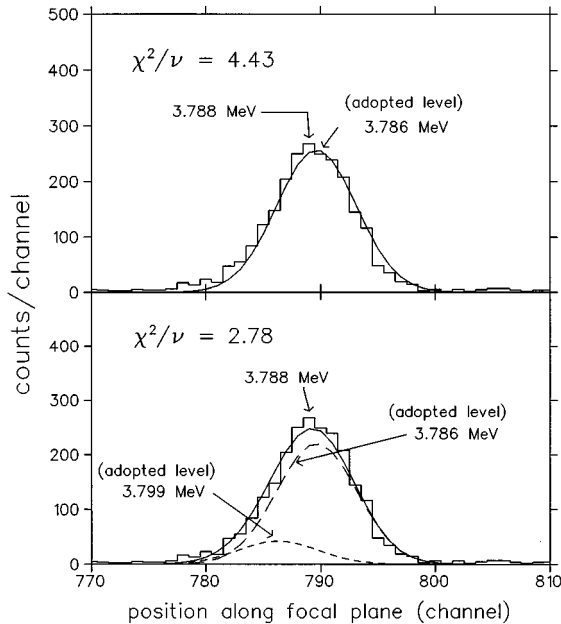


FIG. 15. (top) A fit to the ⁵⁴Cr peak observed at an excitation energy of 3.788 MeV using a Gaussian line shape. (bottom) A fit to the same peak using two Gaussian functions. The solid curve represents a superposition of these Gaussians. See text for discussion.

same region of the spectrum. In this case a χ^2/ν of 2.78 was obtained. The fit obtained is also shown in Fig. 15. Although the reduced χ^2 was lower using two Gaussians, the FWHM of the superposition of the two Gaussians was larger than average for this run. Since the FWHM of the superposition fell within three standard deviations of the average, however, it is possible that the 3.799 MeV (4^+) state is excited. Using the fits described above, it was possible to establish an upper limit on the intensity of the state at 3.799 MeV relative to that at the 3.786 MeV. This intensity ratio was found to be $\sim 20:100$. No lower limit on the relative intensities could, however, be established. Curve II in Fig. 14 shows the results of the optimization of χ^2 following the assigning of $\sim 17\%$ of the 5^+ strength associated with the observed 3.788 MeV state to the 4^+ strength associated with the 3.799 MeV state.

Also of interest is that, although the fit to the sum rules shown in curve II of Fig. 14 is much improved over that for curve I, the value of n_{\min} is similar for the two cases. This feature of sum-rule fits has been noted before [2], and implies that the optimal renormalization of the data is robust against possible errors in the data.

With n_{\min} determined in this way, the absolute normalizations n^+ and n^- of the stripping and pickup data of Table VI can be extracted [1], given an estimate of the fraction γ of the total 0f_{7/2} proton strength that resides outside the excitation energy region probed by the transfer experiments. With $n_{\min} = 0.89$ from curve I of Fig. 14 and $\gamma = 0.2 \pm 0.1$ [1], we find that the stripping and pickup data of Table VI should be multiplied by $n^+ = 0.74 \pm 0.09$ and $n^- = 0.83 \pm 0.10$, respectively. The diagonal contributions of the 0f_{7/2} proton orbit to various one-body observables can now be calculated, in particular J_i^c , the contribution to J_i , the maximum z projection of the spin of the ⁵⁵Mn ground state. Using the pickup data of Table VI, for example,

$$J_i^c = \frac{1}{2(J_i + 1)} \sum_{J'} \{J_i(J_i + 1) + j(j + 1) - J'(J' + 1)\} n^- S_{J'}^-, \quad (16)$$

with a similar expression involving the stripping quantities. Taking the average of these two estimates, we find $J_i^c = 2.05 \pm 0.21$. As far as other fp valence orbits are concerned, our results indicate that their contribution to J_i^c is negligible.

Since a fractional increase of $(1 - \gamma)$ generates an identical fractional increase of n^+ and n^- [1], a value of $\gamma \sim 0$ results in $J_i^c = J_i$. Thus, in common with other sum-rule analyses in the lower fp shell [2], the transfer data are consistent with the simple picture in which the 0f_{7/2} orbit is being preferentially filled, with the low-lying spectroscopic strength close to the corresponding shell-model values. This is at odds with the spectroscopic factors for pickup from valence orbits determined using the $(e, e'p)$ reaction on medium mass nuclei [34,35]. Although some enhancement of the latter may be in order [36,37], we should stress here that our determination of $\gamma \sim 0$ is model dependent, in particular in the spin distribution assumed for the unseen strength [1].

V. SUMMARY

Angular distributions associated with the $^{55}\text{Mn}(d, ^3\text{He})^{54}\text{Cr}$ ($E_d = 46$ MeV) reaction have been measured and analyzed to yield spectroscopic factors for 24 final states up to an excitation of 6.104 MeV in ^{54}Cr . Symmetric NEWSR analyses of the $0f_{7/2}$ transfer data, together with comparisons with shell-model results, have allowed us to make spin assignments of 6^+ , 5^+ , and 6^+ to the levels in ^{54}Cr located at 3.222, 3.786, and 4.042 MeV excitation, respectively. For the remaining orbitals of the $0f_{1p}$ shell, our findings are consistent with a small $1p_{3/2}$ and negligible $0f_{5/2}$ and $1p_{1/2}$ proton occupancy in ^{55}Mn . We have also located a substantial fraction of the $0s_{1d}$ proton pickup strength above 4.128 MeV, allowing us to make some further spin and parity assignments, in particular that of 3^- to the 4.245 MeV state of ^{54}Cr .

Our symmetric NEWSR fits, though acceptable, are inferior to those previously obtained for ^{51}V and ^{59}Co [1], pointing to some deficiencies in the $0f_{7/2}$ proton transfer data used. Nevertheless, good overall agreement with the results of a recent shell-model calculation using a new effective interaction for the $0f_{1p}$ shell has been found, emphasizing the reliability of this calculation.

ACKNOWLEDGMENTS

The assistance of D. R. Geduld during the target manufacture and thickness measurement is much appreciated. One of us (R.T.N.) is grateful to the Foundation for Research Development, the University of Cape Town Research Committee, and the Mellon Foundation for financial support received.

-
- [1] R. T. Newman and S. M. Perez, *Phys. Rev. C* **51**, 1414 (1995).
 [2] C. F. Clement and S. M. Perez, *Rep. Prog. Phys.* **54**, 127 (1991).
 [3] P. F. Hinrichsen and B. Rosner, *Bull. Am. Phys. Soc.* **12**, 696 (1967).
 [4] M. Matoba, *Nucl. Phys.* **A118**, 207 (1968).
 [5] Huo Junde, *Nucl. Data Sheets* **67**, 523 (1992).
 [6] Huo Junde, Hu Dailing, Zhou Chunmei, Han Xiaoling, Hu Baohua, and Wu Yaodong, *Nucl. Data Sheets* **51**, 1 (1987).
 [7] L. Colli, I. Iori, S. Micheletti, and M. Pignaneli, *Nuovo Cimento* **20**, 94 (1961).
 [8] L. Colli, F. Cvelber, S. Micheletti, and M. Pignaneli, *Nuovo Cimento* **14**, 1120 (1959).
 [9] J. L. Yntema, T. H. Braid, B. Zeidman, and H. W. Broek, in *Proceedings of the Rutherford Jubilee International Conference*, Manchester, 1961, edited by J. B. Birks (Academic Press, New York, 1961), p. 521.
 [10] G. R. Satchler, *Direct Nuclear Reactions* (Oxford University Press, New York, 1983).
 [11] S. M. Barr and R. M. DelVecchio, *Phys. Rev. C* **15**, 114 (1977).
 [12] H.-J. Trost, A. Schwarz, U. Feindt, F. H. Heimlich, S. Heinzel, J. Hintze, F. Körber, R. Lekebusch, P. Lezoch, G. Möck, W. Paul, E. Roick, M. Wolff, J. Worzeck, and U. Strohhusch, *Nucl. Phys.* **A337**, 377 (1980).
 [13] J. Bojowald, H. Machner, H. Nann, W. Oelert, M. Rogge, and P. Turek, *Phys. Rev. C* **38**, 1153 (1988).
 [14] M. G. van der Merwe, W. A. Richter, and B. A. Brown, *Nucl. Phys.* **A579**, 173 (1994).
 [15] A. H. Botha and H. N. Jungwirth, in *Proceedings of the Tenth International Conference on Cyclotrons and their Applications*, Michigan, 1984, edited by F. Marti (IEEE, New York, 1984), p. 263.
 [16] J. V. Pilcher, A. A. Cowley, D. M. Whittal, and J. J. Lawrie, *Phys. Rev. C* **40**, 1937 (1989).
 [17] G. P. A. Berg, L. Bland, C. C. Foster, J. Lisanti, T. Rinckel, R. Sawafta, P. Schwandt, K. Solberg, and E. J. Stephenson, Scientific and Technical Report, Indiana University Cyclotron Facility, 1988-1989, p. 200.
 [18] L. R. Doolittle, *Nucl. Instrum. Methods B* **9**, 344 (1985).
 [19] J. W. Müller, *Nucl. Instrum. Methods* **163**, 241 (1979).
 [20] C. R. Gould, L. G. Holzswig, S. E. King, Y. C. Lau, R. V. Poore, N. R. Roberson, and S. A. Wender, *IEEE Trans. Nucl. Sci.* **NS-28**, 3708 (1981).
 [21] J. V. Pilcher, Internal Report, National Accelerator Center, 1988.
 [22] W. Bertozzi, M. V. Hynes, C. P. Sargent, C. Creswell, P. C. Dunn, A. Hirsch, M. Leitch, B. Norum, F. N. Rad, and T. Sasanuma, *Nucl. Instrum. Methods* **141**, 457 (1977).
 [23] F. Neumeyer and S. Strauch, computer program FIT2.1, Technische Hochschule Darmstadt (unpublished).
 [24] J. B. Marion and F. C. Young, *Nuclear Reaction Analysis* (North-Holland, Amsterdam, 1968).
 [25] Xi-Ting Lu, *Nucl. Instrum. Methods* **225**, 283 (1984).
 [26] Wang Gongqing, Zhu Jiabi, and Zhang Jingen, *Nucl. Data Sheets* **50**, 255 (1987).
 [27] Huo Junde, Sun Huibin, Zhao Weizhong, and Zhou Qing, *Nucl. Data Sheets* **68**, 887 (1993).
 [28] F. James and M. Roos, *Comput. Phys. Commun.* **10**, 343 (1975).
 [29] P. D. Kunz and E. Rost, in *Computational Nuclear Physics 2—Nuclear Reactions*, edited by K. Langanke, J. A. Maruhn, and S. E. Koonin (Springer-Verlag, New York, 1993), p. 88.
 [30] N. Austern, R. M. Drisko, E. C. Halbert, and G. R. Satchler, *Phys. Rev.* **133**, B3 (1964).
 [31] C. F. Clement and S. M. Perez, *Nucl. Phys.* **A284**, 469 (1977).
 [32] P. Schwandt, "SNOOPY8 - Optical Potential Code for Elastic Scattering Analysis," Report No. 82-3, Indiana University Cyclotron Facility, 1982.
 [33] J. Verotte, G. Berrier-Ronsin, S. Fortier, E. Hourani, J. Kalifa, A. Khendriche, J. M. Maison, L. H. Rosier, and G. Rotbard, *Phys. Rev. C* **49**, 1559 (1994).
 [34] G. J. Kramer *et al.*, *Phys. Lett. B* **227**, 199 (1989).
 [35] J. W. A. den Herder, H. P. Blok, E. Jans, P. H. M. Keizer, L. Lapikás, E. N. M. Quint, G. van der Steenhoven, and P. K. A. de Witt Huberts, *Nucl. Phys.* **A490**, 507 (1988).
 [36] J. M. Udías, P. Sarriguren, E. Moya de Guerra, E. Garrido, and J. A. Caballero, *Phys. Rev. C* **51**, 3246 (1995).
 [37] J. M. Udías, P. Sarriguren, E. Moya de Guerra, E. Garrido, and J. A. Caballero, *Phys. Rev. C* **48**, 2731 (1993).